Millimeter-Wave Wideband and Wide-Angle Scanning Phased Array Antenna Using Simple Scanning Enhancement Method

Peidong Feng, Wanchen Yang, *Senior Member, IEEE*, Qiaguang Liu, Wenquan Che, *Fellow, IEEE*, and Shilong Pan, *Fellow, IEEE*

***Abstract*—This letter presents a millimeter-wave (mmWave) wideband and wide-angle scanning phased array antenna using a simple scanning enhancement method for small-scale array. First, introducing a stepped ground (SG) can significantly broaden 3 dB beamwidth of the magnetoelectric (ME) dipole antenna element. Based on the wide-beam element, a 4 × 4 array is constructed with a spacing of only 0.378λ_0 (at 27 GHz), and with SG, high frequency scanning gain improves by 6 dB, achieving a 61° max scan angle with no gain loss. To further enhance the scanning performance of the phased array, a metasurface structure (MS) is integrated, extending the scanning angle from 61° to over 66° and increasing the maximum scanning angle to 69°. Additionally, π-shaped and X-shaped decoupling paths are introduced to effectively reduce the coupling between adjacent elements as well as between nonadjacent elements. This approach enhances isolation, improves active *S*-parameter performance, and boosts efficiency. Fabricated using low-temperature co-fired ceramics (LTCC) technology, the antenna achieves a wide bandwidth of 24 GHz to 29.5 GHz, covering 5G n257 and n258 bands, with a scanning range exceeding ±66°, and a gain fluctuation within 3 dB. Additionally, the coupling coefficient remains below −19.5 dB, while the active *S*-parameter stays below −10.3 dB at maximum scanning angles, and the efficiency surpassing 70%.**

***Index Terms*—Decoupling, magnetoelectric (ME) dipole, metasurface, phased array, wide-beam elements.**

I. Introduction

MILLIMETER-WAVE (mmWave) frequency band, as a crucial component of 5G and 6G frequencies, offers advantages such as large bandwidth, large communication capacity, beam concentration, high transmission rates, and low latency, making it better suited to meet the demands of modern applications [1], [2], [3]. Meanwhile, mmWave, characterized by high frequencies and short wavelengths, faces challenges such as high path loss, significant signal attenuation, and limited coverage. Phased array antennas address these issues by controlling the phase and amplitude of array elements to achieve multibeam coverage, effectively mitigating these limitations [4], [5], [6], [7]. However, existing mmWave phased array technologies are still constrained by a small beam-scanning area and degradation of radiation patterns, such as significant gain fluctuations, high sidelobes, and mismatches, which hinder their practical applications [8].

To improve the wide-angle scanning performance and expand the beam-scanning range of mmWave phased array antennas, several studies have been conducted. For example, some approaches focus on broadening the beamwidth of antenna elements [8], [9], [10], constructing pattern-reconfigurable antennas [11], [12], [13], or employing tightly coupled elements [14]. However, pattern-reconfigurable antennas suffer from high losses and instability of switching components at mmWave frequencies, while tightly coupled elements result in low antenna efficiency and fabrication challenges. Therefore, broadening the beamwidth of antenna elements remains a commonly used approach for mmWave phased arrays. In addition, closely spaced antenna elements are prone to strong coupling, which degrades scanning performance. Decoupling has thus become a critical research focus [15], [16], [17], [18]. For example, in [16], decoupling between antennas was achieved using a decoupling surface. By placing a decoupling surface above the array, effective decoupling is realized. This method is simple and applicable to various antenna types. In [18], an effective decoupling technique based on planar coupling cancellation was proposed, introducing an additional coupling path with equal magnitude and opposite phase to cancel the inherent coupling

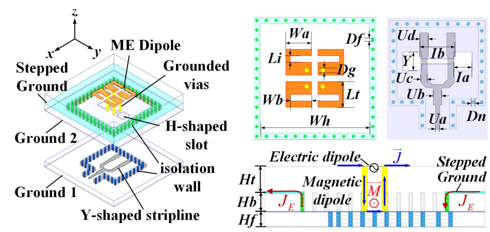

Fig. 1. Topology of the proposed wide-beam ME antenna element: (a) 3-D view and (b) top view and side view. ($Wa = 0.8$mm, $Wb = 0.6$ mm, $Lt = 0.8$ mm, $Li = 0.2$ mm, $Wh = 3.4$ mm, $Ua = 0.12$ mm, $Ub = 0.25$ mm, $Uc = 0.19$ mm, $Ud = 0.25$ mm, $Ia = 0.54$ mm, $Ib = 0.95$ mm, $Y = 0.55$ mm, $Hf = 0.376$ mm, $Hb = 0.47$ mm, $Ht = 0.658$ mm, $Dg = 0.15$ mm, $Df = 0.1$ mm, $Dn = 0.1$ mm.)

Received 13 June 2025; revised 29 June 2025; accepted 4 July 2025. Date of publication 8 July 2025; date of current version 1 December 2025. This work was supported in part by the National Key R&D Program of China under Grant 2022YFB2802704 and in part by the National Natural Science Foundation of China under Grant 62471219 and Grant 62321002. *(Wanchen Yang and Shilong Pan contributed equally to this work.) (Corresponding author: Wanchen Yang.)*

Peidong Feng, Wanchen Yang, and Shilong Pan are with the College of Electronic and Information Engineering, Nanjing University of Aeronautics and Astronautics, Nanjing 211106, China (e-mail: wcyang@nuaa.edu.cn).

Qiaguang Liu and Wenquan Che are with the Guangdong Key Laboratory of Millimeter-Waves and Terahertz, School of Electronic and Information Engineering, South China University of Technology, Guangzhou 510641, China.

Digital Object Identifier 10.1109/LAWP.2025.3586946

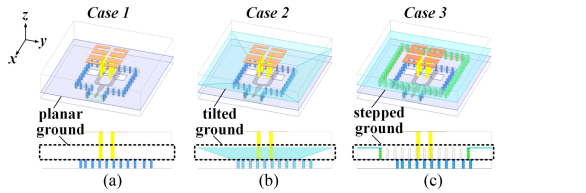

Fig. 2. Antenna element with three different ground planes: (a) *Case 1* (planar ground), (b) *Case 2* (tilted ground), and (c) *Case 3* (stepped ground).

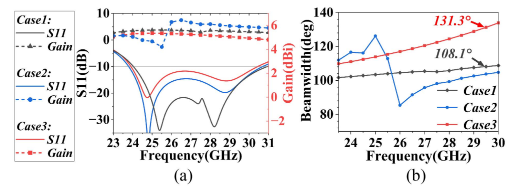

Fig. 3. Performances of the antenna element for three cases: (a) S_{11} and gain of *Case 3*, (b) 3 dB beamwidths.

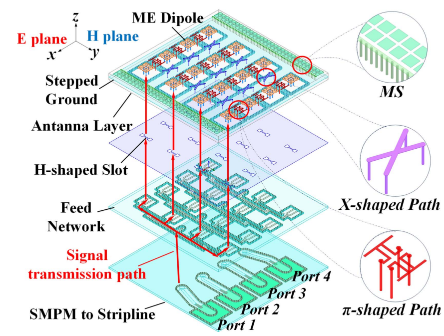

Fig. 4. Configuration of the proposed phased array antenna.

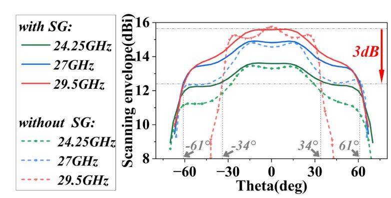

Fig. 5. Scanning envelope of the phased array with and without the SG.

paths. This approach adds no extra profiles, which makes it be fabrication-friendly and suit wideband applications.

Inspired by the above works, a mmWave wideband and wide-angle scanning phased array antenna using a simple scanning enhancement method for small-scale array is presented. A stepped ground (SG) and metasurface structure (MS) are used to widen the beamwidth of the ME dipole element, improving scanning performance in a 4×4 array. Additionally, π-shaped and X-shaped decoupling paths are introduced to respectively reduce the couplings between adjacent elements or between non-adjacent elements, for improving active *S*-parameters and boosting efficiency.

II. Wide-Beam Magnetoelectric Dipole Antenna Element Based on Stepped Ground

Due to the broadband impedance matching characteristics of the ME dipole, a broadband antenna element based on the ME dipole is proposed, as shown in Fig. 1. The design features four rectangular metallic patches with slots and four grounded vias. To enhance bandwidth, the ME dipole is fed by a Y-shaped stripline coupled through an H-shaped slot etched on the ground, specifically designed for optimal impedance matching. Additionally, to mitigate energy leakage, an isolation wall composed of metal grounded vias and metal strips is placed around the stripline. The antenna substrate is LTCC ($\varepsilon_r = 5.9$, tanδ = 0.002), and the metallic patches above the ground plane serve as an electric dipole, while the metal ground vias connect the ground plane to the patches, forming a magnetic dipole, as shown in Fig. 1(b).

As we know, the ground of an antenna often functions as its reflector. By modifying its structure, the reflection paths can be adjusted, thereby altering the antenna's gain and shaping radiation beams with specific characteristics. Similarly, structural modifications to the ground can redistribute the antenna's energy, enhancing radiation performance at low elevation angles and subsequently broadening the beamwidth. Fig. 2 illustrates mmWave antenna elements with three different types of ground reflectors. In *Case 1*, a standard planar ground is used. In *Case 2*, resembling a parabolic antenna, a tilted ground is used to concentrate energy. *Case 3* employs the SG, redistributing energy to improve radiation performance at low elevation angles.

The performance of the proposed wide-beam antenna with the SG is illustrated in Fig. 3. It operates within a bandwidth of 24 GHz to 29.5 GHz (20.6%), covering 5G n257 and n258 bands, with a maximum gain of 5.34 dB. The addition of the SG enhances the antenna's beamwidth across the 5G n257 and n258 bands, particularly at higher frequencies (such as 29.5 GHz), where the proposed antenna element in *Case 3* achieves a 3 dB beamwidth of 131.3°, an increase of 23.2° compared to the element without the SG. As a result, the 3 dB beamwidth in the whole band is over 110°.

III. Wideband and Wide-Angle Scanning Phased Array Antenna Using Simple Scanning Enhancement Method

Based on the above wide-beam ME dipole element, a 4×4 phased array is designed, as shown in Fig. 4, where every four ME dipole elements along the H-plane direction form a subarray, which is fed by a 1-to-4 power divider. The subarrays are arranged along the E-plane direction with an interelement spacing of 4.2 mm ($0.378\lambda_0$ at 27 GHz). The use of an interelement spacing smaller than half a wavelength effectively suppresses grating lobes, thereby achieving improved scanning performance. Additionally, by integrating MS and decoupling paths, the phased array antenna further enhances scanning performance, isolation, and efficiency.

A. Scanning Enhancement via Wide-Beam ME Dipole Element by Loading Stepped Ground

To clearly illustrate the improvement in scanning performance provided by the SG, Fig. 5 presents the scanning envelopes at different frequencies, both with and without the SG. The inclusion of the SG significantly enhances the phased array scanning capability.

Notably, gain attenuation is reduced after incorporating the SG, with the improvement being particularly pronounced at higher frequencies and larger scan angles. For instance, as indicated by the 3 dB gain drop contour in the figure, the scanning range has been significantly expanded from ±34° to ±61° at 29.5 GHz without any gain reduction at the peak. Additionally, the gain performance across scanning envelopes at other

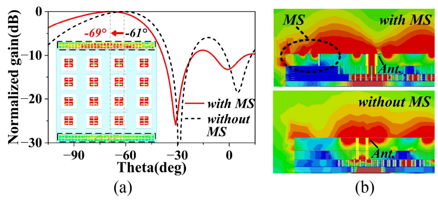

Fig. 6. Performance of the phased array with and without MS at 29.5 GHz. (a) Radiation patterns when scanning to max angle. (b) Electric field.

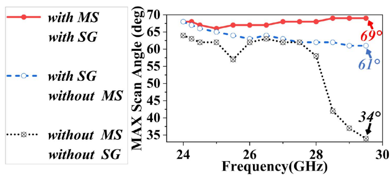

Fig. 7. Scanning performance with and without the MS or SG.

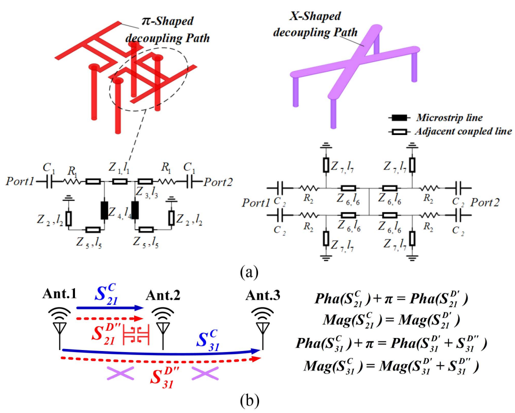

Fig. 8. (a) Equivalent circuits ($R_1 = 190\ \Omega$, $C_1 = 24$ fF, $R_2 = 225\ \Omega$, $C_2 = 57$ fF) and (b) decoupling principle of the MPCCP.

frequencies is improved, with the maximum scanning angle at each frequency point exceeding 61°, effectively expanding the phased array's scanning range.

B. Scanning Enhancement via Metasurface Structure

To further enhance the scanning performance, MS are loaded on both sides of the phased array, as shown in Fig. 4. The MS consists of metasurfaces and metal grounded vias. By appropriately adjusting the position and size of the MS, surface waves can be guided to radiate at the edges of the array. This is because the periodic metasurfaces can excite higher-order harmonics, enabling the transformation of the reference surface into a radiated wave in free space—allowing the slow wave to radiate [19]. This improvement enhances the low-elevation radiation performance of the edge elements, thereby broadening the beamwidth of the array elements.

Fig. 6(a) illustrates the scanning performance at 29.5 GHz before and after integrating the MS. It is evident that the maximum scanning angle of the beam extends from $-61°$ to $-69°$, significantly broadening the scanning range of the phased array. Fig. 6(b) presents the electric field distributions of the 4×4 phased array with and without the MS. It can be observed that, after incorporating the MS, the electric field at the array edges is significantly enhanced. The electric field distribution of the upper MS is similar to that of the radiation patches, indicating

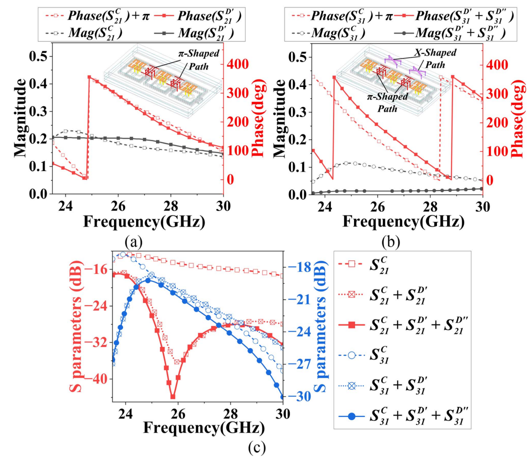

Fig. 9. (a) Magnitude and phase of S_{21}^{C} and $S_{21}^{D'}$. (b) Magnitude and phase of $S_{31}^{D'}$ and $S_{31}^{D''}$. (c) S-parameters with and without MPPCP.

that the upper MS enhances the scanning angle in the negative direction, while the lower MS improves the scanning angle in the positive direction.

To highlight the impact of the MS on expanding the maximum scanning angle of the phased array, Fig. 7 shows the maximum scanning angle at different frequencies with and without the MS and SG. This figure further demonstrates, from another perspective, that with SG, the scanning angle increases from 34° to 61°. Subsequently, the MS further enhances the scanning performance of the phased array, extending the scanning angle from 61° to over 66° at the whole bands, and increasing the maximum scanning angle to 69°, with gain fluctuation controlled within 3 dB.

C. High Isolation and Low Active S-Parameters via Multiple Decoupling Structures

As shown in Fig. 4, to address the coupling issues in the 0.378 λ_0-spaced phased array, π-shaped and X-shaped paths, perceived as multiple planar coupling cancellation paths (MPCCP), are introduced between elements, whose equivalent circuits are presented in Fig. 8(a). The closely spaced metal segments are modeled as coupled lines, shorter segments as microstrip lines, and radiation resistance and coupling capacitors are included to represent radiated energy and antenna-structure interaction, respectively [18]. Fig. 8(b) illustrates a three-element array to demonstrate the decoupling principle of the MPCCP. The inherent coupling between adjacent and non-adjacent elements is denoted as S_{21}^{C} and S_{31}^{C}, while the coupling introduced by the π-shaped path is represented as $S_{21}^{D'}$ and $S_{31}^{D'}$ and the coupling introduced by X-shaped path is represented as $S_{21}^{D''}$ and $S_{31}^{D''}$, respectively. The magnitude and phase of S_{21}^{C} and S_{31}^{C} are obtained from a three-element array without MPCCP, while $S_{21}^{D'}$, $S_{21}^{D''}$, $S_{31}^{D'}$, and $S_{31}^{D''}$ are derived from the MPCCP equivalent circuits. The MPCCPs generate equal-magnitude and anti-phase coupling that effectively cancel the array's inherent coupling, resulting in improved array performance.

As shown in Fig. 9(a), the π-shaped path generates equal-amplitude, 180° phase-inverted coupling to cancel inherent coupling, achieving over 15 dB S_{21} reduction in 25 GHz to 29.5 GHz and 5 dB to 10 dB in 24 GHz to 25 GHz in Fig. 9(c). However, note that S_{31} slightly deteriorates at higher frequencies. To

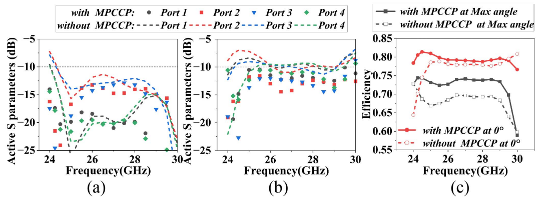

Fig. 10. Active *S*-parameters and efficiency of the array with/without MPCCP: (a) Active *S*-parameters scanning at 0°, (b) active *S*-parameters scanning at maximum angle, and (c) antenna efficiency.

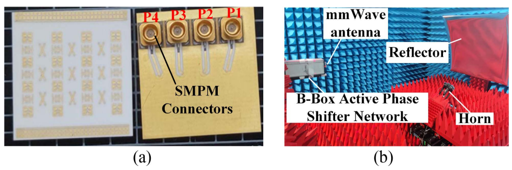

Fig. 11. (a) Fabricated 4 × 4 phased array prototype and (b) testing environment for phased array's radiation performance.

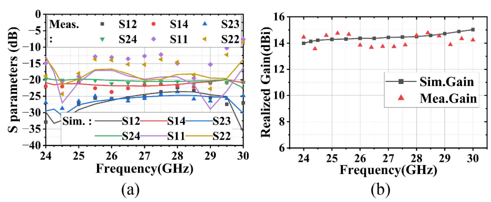

Fig. 12. Measured and simulated results of the proposed array: (a) *S*-parameter curves and (b) gain curves.

mitigate this, X-shaped paths are added in Fig. 9(b), creating cancellation ($S_{31}^{D'} + S_{31}^{D''}$) that reduces S_{31} by 4 dB at high frequencies without impacting S_{21} in Fig. 9(c).

Due to the improved isolation, the active *S*-parameters at the maximum scanning angle were enhanced. Fig. 10 illustrates active *S*-parameters and efficiency of the antenna with and without decoupling paths. The active *S*-parameter when scanning at 0° has been improved by decoupling especially at lower frequencies, while the active *S*-parameter when scanning at the maximum scanning angle has significantly declined from −6.9 dB to −10.3 dB in the whole band. Additionally, the decoupling effect enhanced antenna efficiency to over 78.8% for scanning at 0°, while the efficiency remains above 70% for the maximum scanning angle.

IV. Results and Discussions

To demonstrate the performance of the proposed phased antenna array using 4 × 4 wide-beam antenna elements, a prototype was fabricated, as shown in Fig. 11(a), with four SMPM connectors soldered to the back of the antenna at four ports. These connectors excite the antenna via grounded coplanar waveguide (GCPW) transmission lines. The *S*-parameter measurements were carried out with a vector network analyzer (VNA), and the results are shown in Fig. 12(a). Within the 24 GHz to 29.5 GHz bandwidth (20.6%), the reflection coefficient remains below −10 dB, while the coupling coefficient stays below −19.5 dB. For adjacent subarrays, the coupling coefficient remains below −22 dB across the same frequency range.

The radiation pattern performance of the phased array was tested in a compact range chamber, as shown in Fig. 11(b). The scanning performance of the phased array is shown in Fig. 13

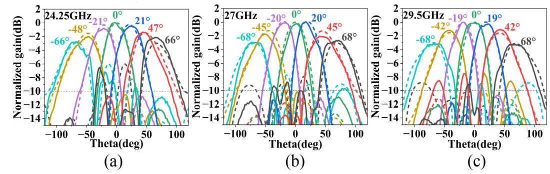

Fig. 13. 4 × 4 phased array scanning performance. (a) 24.25 GHz, (b) 27 GHz, and (c) 29.5 GHz.

TABLE I
Scanning Performance of the Proposed Phased Array

Freq.	Scan angle (deg) (Sim. / Meas.)	Gain variation (dB) (Sim. / Meas.)
24.25GHz	±66 / ±66	3.0 / 2.7
27GHz	±68 / ±70	3.0 / 3.0
29.5GHz	±68 / ±68	3.0 / 3.2

TABLE II
Comparison With Other Millimeter-Wave Phased Arrays

Ref.	Bandwidth (GHz)	Number (Spacing)	Isolation (dB)	Scanning angle (deg)	Gain variation (dB)
[8]	24.25-29.5 (19.5%)	4×4 (0.45 λ_0)	⩾21	>±55	3
[18]	25-29.5 (16.5%)	4×4 (0.45 λ_0)	⩾20	>±55	3
[20]	27.1-29.4 (8.1%)	4×4 (0.57 λ_0)	⩾15	⩾±45	3
[21]	22.8-24.1 (5.5%)	4×4 (0.5 λ_0)	⩾12.5	⩾±60	3
[22]	24-34 (34.5%)	8×8 (0.5 λ_0)	-	⩾±60 (24-31.5GHz)	4.6
This work	24-29.5 (20.6%)	4×4 (0.378 λ_0)	⩾19.5	⩾±66	3

and Table I. Fig. 13 presents the normalized test results of the phased array's scanning performance at 24.25 GHz, 27 GHz, and 29.5 GHz. Across 24 GHz to 29.5 GHz, the scanning range of the phased array exceeds ±66°, reaching a maximum of ±68°, and gain loss within 3 dB. In the figure, the dashed lines represent the simulated scanning performance, while the solid lines indicate the measured results. Accounting for fabrication and testing errors, the measured results align closely with the simulations in terms of scanning gain, scan angle, and beamwidth during scanning. In addition, Fig. 12(b) shows the measured and simulated gain curves of the phased array, which are acceptable within a certain margin of error.

Table II compares the proposed scanning array with other related studies. It is evident that, under the same array scale, the proposed phased array antenna exhibits the widest scanning range up to ±66° within 3 dB gain fluctuation in the whole band of 5G n257 and n258 bands; meanwhile, it offers a higher isolation in the smallest element space.

V. Conclusion

This work demonstrates a mmWave wideband, wide-angle scanning phased array antenna using simple scanning enhancement method for small-scale array. With the integration of the SG, MS, and MPCCP, the array achieves a broadband covering 24 GHz to 29.5 GHz, a very large scanning range exceeding ±66°. Additionally, the antenna exhibits a low coupling coefficient, along with favorable active *S*-parameters and high efficiency. Fabrication and testing validate the design, demonstrating its suitability for mmWave applications.

References

[1] W. Hong, K.-H. Baek, and S. Ko, "Millimeter-wave 5G antennas for smartphones: Overview and experimental demonstration," *IEEE Trans. Antennas Propag.*, vol. 65, no. 12, pp. 6250–6261, Dec. 2017.

[2] Q. Luo et al., "Design and analysis of a reflectarray using slot antenna elements for Ka-band SatCom," *IEEE Trans. Antennas Propag.*, vol. 63, no. 4, pp. 1365–1374, Apr. 2015.

[3] L. Wei, W. Yang, Q. Xue, and W. Che, "Aperture-shared design of millimeter-wave phased array and sub-6 GHz antenna using diversified metasurface structures," *IEEE Trans. Antennas Propag.*, vol. 72, no. 8, pp. 6362–6373, Aug. 2024.

[4] J. Helander, K. Zhao, Z. Ying, and D. Sjöberg, "Performance analysis of millimeter-wave phased array antennas in cellular handsets," *IEEE Antennas Wireless Propag. Lett.*, vol. 15, pp. 504–507, 2016.

[5] Z. Qu, S.-W. Qu, Z. Zhang, S. Yang, and C. H. Chan, "Wide-angle scanning lens fed by small-scale antenna array for 5G in millimeter-wave band," *IEEE Trans. Antennas Propag.*, vol. 68, no. 5, pp. 3635–3643, May 2020.

[6] X. Gu, D. Liu, and B. Sadhu, "Packaging and antenna integration for silicon-based millimeter-wave phased arrays: 5G and beyond," *IEEE J. Microw.*, vol. 1, no. 1, pp. 123–134, Jan. 2021.

[7] H. Gao et al., "Design and experimental validation of automated millimeter-wave phased array antenna-in-package (AiP) experimental platform," *IEEE Trans. Instrum. Meas.*, vol. 70, 2021, Art. no. 8000711.

[8] D. Chen, W. Yang, S. Pan, Q. Xue, and W. Che, "Millimeter-wave 45°-polarized LTCC phased array using wide-beam patch-via-wall elements for wide-angle scanning applications," *IEEE Trans. Antennas Propag.*, vol. 71, no. 12, pp. 9497–9508, Dec. 2023.

[9] N.-W. Liu, L. Zhu, Z.-X. Liu, and Y. Liu, "Dual-band single-layer microstrip patch antenna with enhanced bandwidth and beamwidth based on reshaped multiresonant modes," *IEEE Trans. Antennas Propag.*, vol. 67, no. 11, pp. 7127–7132, Nov. 2019.

[10] M. Li and K.-M. Luk, "Wideband magneto-electric dipole antenna for 60-GHz millimeter-wave communications," *IEEE Trans. Antennas Propag.*, vol. 63, no. 7, pp. 3276–3279, Jul. 2015.

[11] Y.-Y. Bai, S. Xiao, M.-C. Tang, Z.-F. Ding, and B.-Z. Wang, "Wide-angle scanning phased array with pattern reconfigurable elements," *IEEE Trans. Antennas Propag.*, vol. 59, no. 11, pp. 4071–4076, Nov. 2011.

[12] X. Ding, Y.-F. Cheng, W. Shao, H. Li, B.-Z. Wang, and D. E. Anagnostou, "A wide-angle scanning planar phased array with pattern reconfigurable magnetic current element," *IEEE Trans. Antennas Propag.*, vol. 65, no. 3, pp. 1434–1439, Mar. 2017.

[13] V. Suryapaga and V. V. Khairnar, "Review on multifunctional pattern and polarization reconfigurable antennas," *IEEE Access*, vol. 12, pp. 90218–90251, 2024.

[14] H. Zhang, S. Yang, Y. Chen, J. Guo, and Z. Nie, "Wideband dual-polarized linear array of tightly coupled elements," *IEEE Trans. Antennas Propag.*, vol. 66, no. 1, pp. 476–480, Jan. 2018.

[15] Y.-F. Cheng, X. Ding, G.-F. Gao, W. Shao, and C. Liao, "Analysis and design of wide-scan phased array using polarization-conversion isolators," *IEEE Antennas Wireless Propag. Lett.*, vol. 18, no. 3, pp. 512–516, Mar. 2019.

[16] K.-L. Wu, C. Wei, X. Mei, and Z.-Y. Zhang, "Array-antenna decoupling surface," *IEEE Trans. Antennas Propag.*, vol. 65, no. 12, pp. 6728–6738, Dec. 2017.

[17] T. Pei, L. Zhu, J. Wang, and W. Wu, "A low-profile decoupling structure for mutual coupling suppression in MIMO patch antenna," *IEEE Trans. Antennas Propag.*, vol. 69, no. 10, pp. 6145–6153, Oct. 2021.

[18] L. Gu, W. Yang, S. Liao, Q. Xue, and W. Che, "Novel coupling cancellation method by loading planar path for wideband high-isolation wide-scanning millimeter-wave phased array," *IEEE Trans. Antennas Propag.*, vol. 70, no. 11, pp. 10520–10530, Nov. 2022.

[19] D. R. Smith et al., "Gradient index metamaterials," *Phys. Rev. E*, vol. 71, 2005, Art. no. 036609.

[20] T. Y. C. M., H. N. G. G., and T. Y. S. R., "A 2-by-2 sub-array for scalable 28 GHz mmWave phased array horn antenna in 5G network," in *Proc. 13th Eur. Conf. Antennas Propag.*, Krakow, Poland, 2019, pp. 1–5.

[21] Z. Yi et al., "A wide-angle beam scanning antenna in E-plane for K-band radar sensor," *IEEE Access*, vol. 7, pp. 171684–171690, 2019.

[22] L. Zhao, Y. Li, M. Chen, and J. Wang, "A millimeter-wave wideband dual-polarized magnetoelectric dipole phased array with scan blindness mitigation," *IEEE Trans. Antennas Propag.*, vol. 72, no. 9, pp. 6875–6885, Sep. 2024.